

MODIFICATION AND DEVELOPMENT OF NEW TYPES OF TEMs








Article

Received: 27 May 2025 | Revised: 5 September 2025 |

Accepted: 9 September 2025 | Published online: 21 September 2025

UDC 66.081.6-278

<https://doi.org/10.31489/2959-0663/3-25-9>

Angelina V. Kryukova-Seliverstova¹, Oleg L. Orelovich², Vladimir A. Altynov²,
Alexander V. Akimov³, Alexander S. Shmakov³, Daria V. Nikolskaya²,
Nikita S. Kirilkin², Uliana V. Pinaeva^{2*}

¹Dubna State University, Dubna, Russia;

²Flerov Laboratory of Nuclear Reactions, Joint Institute for Nuclear Research, Dubna, Russia;

³Federal Research Center of Problems of Chemical Physics and Medicinal Chemistry RAS, Chernogolovka, Russia

(*Corresponding author's e-mail: pinaeva@jinr.ru)

Radiation Grafting of PVDF Track-Etched Membranes: A Study for Nanoscale Pore Functionalization

Functionalization of nanoporous membranes poses a substantial challenge in the development of advanced materials for selective transport applications. The primary objective of this study is to optimize the grafting process to ensure the functionalization is localized onto nanopore walls. Poly(vinylidene fluoride) (PVDF) foils were irradiated with Xe ions (1.2 MeV/u) followed by subsequent etching under optimized conditions to create nanoporous membranes. Radiation grafting of acrylic acid (AA) monomer was performed through the residual radical sites in post-etched pore walls of ion-irradiated PVDF. Radical concentrations after irradiation were quantified using EPR spectroscopy. Examination of reaction parameters including inhibitor concentration, temperature, monomer concentration, and reaction kinetics was conducted to achieve selective grafting within the nanopores. FT-IR and XPS analyses confirmed the successful covalent attachment of poly(acrylic acid) (PAA) to the PVDF TMs. Structural transformations of the PVDF matrix throughout the functionalization process were revealed by DSC analysis. The versatility of the approach was further demonstrated by grafting of pH-responsive poly(4-vinylpyridine), enabling modulation of nanopore surface charge, as evidenced by zeta-potential measurements. The spatial localization of the grafted polymer was confirmed by confocal fluorescence microscopy, demonstrating the potential for creating advanced functional membranes for separation and sensing applications.

Keywords: swift heavy ions, track-etched membranes, polyvinylidene fluoride, radiation grafting, acrylic acid, nanoporous membranes, pore functionalization, ion-irradiated

Introduction

Radiation-induced grafting offers a versatile approach for tailoring polymer properties by creating active sites for monomer polymerization using ionizing radiation. Its adaptability to various polymers, monomers, and reaction conditions, through methods like direct, pre-irradiation, or peroxidation grafting, allows for tailoring of functionalities, such as hydrophilicity or chemical reactivity, onto surfaces or within the bulk material without requiring any contaminating reagents [1].

Poly(vinylidene fluoride) (PVDF) is a fluoropolymer that has garnered significant attention due to its excellent mechanical strength, thermal stability, chemical resistance, and electroactive properties [2]. The development of nanostructured and functionalized PVDF materials is particularly important as it strengthens these inherent properties while introducing new functionalities [3]. For instance, creating nanoporous PVDF membranes through swift heavy ion (SHI) irradiation followed by chemical etching allows for precise tuning

of pore size and geometry [4]. Subsequent functionalization of these nanopores through grafting imparts customized surface chemistries, enhancing performance in applications requiring high selectivity and controlled transport, such as advanced sensors, responsive biomedical implants, and proton-exchange membranes [5, 6].

Radiation grafting of vinyl monomers onto fluoropolymers has been extensively explored since Chapiro's seminal works in the 60s [7, 8]. Studies on radiation grafting of hydrophilic monomers, including acrylic acid (AA), onto polytetrafluoroethylene (PTFE) films to create permselective membranes, highlighted the challenges in controlling homopolymerization and the importance of solvent selection [9]. Ellinghorst et al. [10] described radiation-initiated grafting on PVDF films with AA, emphasizing the importance of achieving "grafting through" for homogeneous membrane properties. More recent studies by Betz, Clochard, Mazzei, and colleagues [11–14] have focused on grafting of styrene and (meth)acrylates onto PVDF, using electron-beam irradiated foils and SHI-etched tracks in PVDF. These works have investigated the influence of monomer concentration, inhibitor presence, and the role of water in achieving surface or grafting through. Mazzei et al. [15] and Cuscito et al. [16] specifically reported on AA grafting onto etched ion tracks in PVDF, demonstrating that residual active sites within the pores can successfully initiate graft polymerization reaction. The method was later enhanced by Barsbay et al. [17], employing RAFT-mediated radical polymerization to graft poly(acrylic acid) (PAA) into the nanochannel walls of track-etched PVDF for the controlled adjustment of nanopore size. Although these studies successfully demonstrated the feasibility of pore grafting approach, a comprehensive optimization of key radiation grafting parameters is still needed for further development of functional membranes.

The present study aims to investigate the radiation-induced graft polymerization process of AA monomer within the nanopores of PVDF track-etched membranes (TMs), built upon the established methodology of initiation through the residual active sites. Radical concentration after irradiation with xenon ion beam was quantified using EPR spectroscopy. A refined chemical etching protocol is reported, achieving a substantial decrease in oxidizer utilization. The effects of key variables on the grafting yield were examined, including inhibitor concentration, monomer concentration, temperature, and reaction kinetics. Covalent attachment of PAA to PVDF TMs was confirmed through FT-IR and XPS analyses, while enhanced hydrophilicity was verified by contact angle measurements. DSC analysis was employed to follow structural changes in PVDF throughout the functionalized membrane fabrication process. Most crucially, localized grafting within nanopores was demonstrated through zeta-potential measurements and confocal fluorescence microscopy. It is anticipated that this work will stimulate further research, thereby providing the basis for the design of advanced materials for use in energy, biomedical, and separation technologies.

Experimental

Materials

A polyvinylidene fluoride (PVDF) film with a thickness of 9 μm was procured from Kureha Chemical Industries Co. Ltd. (Japan). The film exhibited a crystallinity degree of approximately 40 %, as measured by X-ray diffraction (XRD), with the dominant crystalline phase identified as the α -phase and a minor contribution from the β -phase, as confirmed by Fourier-transform infrared (FT-IR) spectroscopy. Functionalized PVDF track-etched membranes (TMs) were synthesized using the following reagents: potassium hydroxide (KOH), potassium permanganate (KMnO_4), sodium metabisulfite ($\text{Na}_2\text{S}_2\text{O}_5$), acrylic acid (AA) monomer, and Mohr's salt ($(\text{NH}_4)_2\text{Fe}(\text{SO}_4)_2 \cdot 6\text{H}_2\text{O}$). To emphasize the localized grafting through zeta-potential assessment, 4-vinylpyridine (4VP) radiation grafting was performed. For photoluminescence (PL) measurements, carboxylic acid activation of PVDF TMs was done to couple ethylenediamine (EDA) using 1-ethyl-3-(3-dimethylaminopropyl)carbodiimide (EDC) and N-hydroxysuccinimide (NHS) prior to grafting with PAA. All chemicals were purchased from Thermo Scientific (USA) and Chemreaktivsnab (Russia), and used as received. Deionized water (Milli-Q, resistivity $\geq 18 \text{ M}\Omega \cdot \text{cm}$) was used for preparing all aqueous solutions.

Swift Heavy Ion (SHI) Irradiation

PVDF foils were irradiated with $^{132}\text{Xe}^{26+}$ ions (1.2 MeV/u) under vacuum using the IC-100 cyclotron at the Flerov Laboratory of Nuclear Reactions, Joint Institute for Nuclear Research (Dubna, Russia). The ion beam was oriented perpendicular to the film surface. The ion fluence, which is related to the resulting track density in the irradiated samples, varied from 10^7 to 10^{10} ions/ cm^2 . The electronic stopping power ($\Delta E_e/\Delta x$) estimation was made with the SRIM-2013. The average electronic energy loss for xenon ions (160 MeV) traversing the PVDF target with a density of 1.78 g/cm^3 was determined to be approximately $77.3 \text{ MeV} \cdot \text{cm}^2/\text{mg}$, which is well above the registration threshold for fluoropolymers [18]. To mitigate post-

irradiation oxidative degradation, all irradiated samples were stored in hermetically sealed containers under a dry nitrogen atmosphere at $-24\text{ }^{\circ}\text{C}$ until further use.

Chemical Etching of Ion Tracks

Chemical etching was performed to remove SHI-degraded material and to transform latent tracks into cylindrical through-nanopores. The process was conducted in an aqueous solution containing 10 M KOH and 0.1 M KMnO_4 at $65\text{ }^{\circ}\text{C}$ for 30 minutes (unless stated otherwise). The diameter of the resulting pores was $45\pm 5\text{ nm}$ as determined by Scanning electron microscopy (SEM). To eliminate residual of KMnO_4 , the track-etched membranes (TMs) were treated with an aqueous solution of $\text{Na}_2\text{S}_2\text{O}_5$ (7.5 % w/v), thoroughly rinsed with deionized water, air-dried at room temperature, and weighted.

Radiation Grafting of Acrylic Acid to PVDF TMs

Radiation grafting reaction of acrylic acid (AA) was performed *via* a pre-irradiation method, initiated by residual trapped radicals remained in PVDF matrix after chemical etching. Most of the grafting experiments were performed on PVDF foils irradiated at the fluence of 10^{10} cm^{-2} (unless stated otherwise). Experimental data is presented as the mean value with error bars representing the standard deviation from at least three independent replicate experiments ($n \geq 3$). Freshly etched TMs were immersed into custom-made glass Schlenk tubes containing an AA monomer solution (with or without Mohr's salt to suppress homopolymerization). In grafting experiments involving the use of Mohr's salt, the latter was grinded in fine powder and was first dissolved in water followed by the addition of AA monomer to yield the needed monomer solution concentration. The monomer solution was purged with argon for 20 minutes to remove dissolved oxygen. The tubes were then hermetically sealed and placed in a thermostated water bath at $60\text{ }^{\circ}\text{C}$ for predetermined reaction times. After polymerization, grafted samples were thoroughly rinsed with deionized water, extracted in a Soxhlet apparatus with $\sim 200\text{ mL}$ of boiling water for 12 hours, dried to constant weight, and weighed. The gravimetric grafting yield (GY) was calculated using equation

$$GY = \frac{m_f - m_0}{m_0} \times 100\%,$$

where m_0 and m_f represent the masses of dry membranes before and after grafting, respectively.

Characterization of PAA-g-PVDF TMs

Radiation grafting of AA to PVDF TMs was monitored by Fourier-Transform Infrared spectroscopy (FT-IR) and X-ray Photoelectron Spectroscopy (XPS). FT-IR spectra were registered in attenuated total reflectance (ATR) and transmission modes on a Nicolet spectrometer (Thermo Scientific) with 32 scans and a resolution of 1 cm^{-1} . XPS spectra were acquired using a Thermo Scientific K-Alpha spectrometer with monochromatic Al $\text{K}\alpha$ X-rays (1486.6 eV , 12 kV , 3 mA). Binding energies were calibrated against the C 1s peak (284.8 eV). Survey scans (100 eV pass energy, 0.5 eV step) and high-resolution spectra (20 eV pass energy, 0.05 eV step) were collected and processed using the Advantage software.

Surface morphology and pore diameters were assessed by Field Emission Scanning Electron Microscopy (FESEM) on a HITACHI SU8020 instrument. Prior to imaging, samples were coated with a 5 nm platinum/palladium layer using a Quorum Q150R magnetron sputtering machine to enhance the sample conductivity. Experimental data is provided as mean values with standard deviations determined from at least 30 pores.

Electron Paramagnetic Resonance (EPR) spectra of Xe-irradiated PVDF foils were recorded using a Bruker ElexSys II E500 X-band spectrometer (9.5 GHz). Samples ($3\text{--}5\text{ mg}$, $\sim 7\times 30\text{ mm}$) were rolled into tubes, sealed in quartz ampoules under argon, and immediately cooled in a liquid nitrogen cryostat. Spectra were acquired between $100\text{--}300\text{ K}$ with a microwave power of 6.325 mW (15 dB attenuation), 100 kHz modulation frequency, and 1 Gauss modulation amplitude.

Photoluminescence (PL) measurements were performed on Rhodamine 6G-adsorbed PAA-g-PVDF TMs using a confocal microscope Ntegra Spectra NT-MDT equipped with a 473 nm laser (0.2 mW) and a $100\times$ objective lens. Scans were recorded over a $10\times 10\text{ }\mu\text{m}^2$ area with number of points of 50 along X and Y axes. Optical images were captured through a camera integrated into the transmission optical path.

Differential scanning calorimetry (DSC) measurements were performed using a Mettler Toledo DSC 3 instrument with aluminum crucibles under dynamic heating conditions from -50 to $200\text{ }^{\circ}\text{C}$ at a rate of $10\text{ }^{\circ}\text{C}/\text{min}$ under nitrogen flow ($10\text{ mL}/\text{min}$).

Contact angle (θ) measurements were conducted using a KRÜSS DSA100 Easy Drop system and Drop Shape Analysis software. Five 3 μL droplets of Milli-Q water were deposited on each sample, and θ values were averaged. All values represent the mean of at least ten independent measurements ($n = 10$).

The membrane zeta-potentials (ζ) before and after radiation grafting of PVDF TMs were assessed through the measurements of streaming potential using a custom-made flow cell. The membrane sample (25 mm in diameter) was clamped between the two cell compartments with Ag/AgCl electrodes positioned on either side of the membrane, ensuring a leak-free seal for the pressure-driven flow. The measurements were carried out in a 0.01 M KCl at pH 3, 5, 6.5, and 8 under applied pressures 0–1 bar and confirmed by three consecutive runs. The ζ -potentials (V) were calculated using the Helmholtz–Smoluchowski equation:

$$\zeta = \frac{k \times \eta}{\varepsilon \times \varepsilon_0} \times \frac{\Delta E}{\Delta P},$$

where k is the electrolyte specific conductivity ($\text{Ohm}^{-1} \cdot \text{m}^{-1}$), η is the electrolyte dynamic viscosity ($\text{Pa} \cdot \text{s}$); ε_0 and ε are the dielectric permittivity of vacuum ($8.854 \times 10^{-12} \text{ C} \cdot \text{V}^{-1} \cdot \text{m}^{-1}$) and the relative permittivity of electrolyte (dimensionless), respectively, $\Delta E/\Delta P$ is the streaming potential-to-pressure gradient ratio (V/Pa).

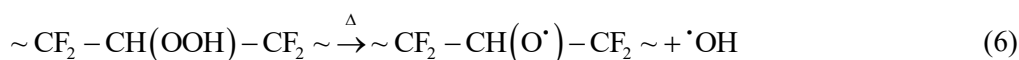
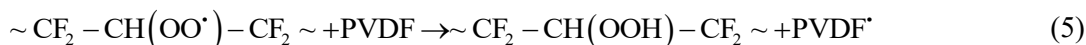
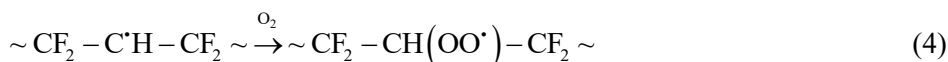
Results and Discussion

SHI-Induced Changes and Generation of Initiators for Graft Polymerization in PVDF

At the ion energy used in this work (1.2 MeV/u), swift heavy ions (SHIs) lose their energy by means of electronic loss processes, but the damage is limited to the ion path. This distinguishes SHI irradiation from electron-beam or γ -rays, where the energy is “homogeneously” distributed. Energy absorption causes excitation and ionization of electrons in the outer shells of atoms, resulting in chemical bond scissions all along the projectile ion pathways. As a primary effect, alkyl in-chain (eq. 1 and 2) and end-chain radicals (eq. 3) are formed



As a result of contact with oxygen, some of the alkyl radicals can undergo oxidation to form peroxy radicals (eq. 4). These peroxy radicals can further form hydroperoxides upon H-abstraction from the PVDF backbone (eq. 5). The hydroperoxides thermally decompose into alkoxy and hydroxyl radicals (eq. 6)



In addition to oxidation, further radical reactions will define the final structure of SHI-irradiated PVDF. These include dehydrofluorination and disproportionation accompanied by the formation of $\text{C}=\text{C}$ bonds, recombination to form cross-links in the polymer and gas molecules (H_2 , F_2 , and HF), H-abstraction, *etc.* Indeed, FT-IR confirmed the appearance of vinylidene groups $-\text{FC}=\text{CH}_2$ and $-\text{HC}=\text{CF}_2$ (1755 cm^{-1}) [19] which were assumed to be a result of main-chain breakage, and $-\text{FC}=\text{CH}-$ (1713 cm^{-1}) as a result of $\text{C}-\text{H}$ scission (*dehydrofluorination*). UV-vis. spectroscopy (not shown) revealed that isolated dienes (absorption maxima at 220 nm) are formed in predominant amounts as a result of radiolysis of PVDF under these irradiation conditions, while the rate of formation of trienes and polyenes is about two and three times slower, respectively.

EPR spectroscopy results for samples irradiated at ion fluences ranging from 10^9 to 3×10^{10} ions/ cm^2 revealed a significant number of radical species centered on the g -factor g_e corresponding to a mixture of polyradicals (Fig. 1 (a)). This is in accordance with observations reported in the literature [20].

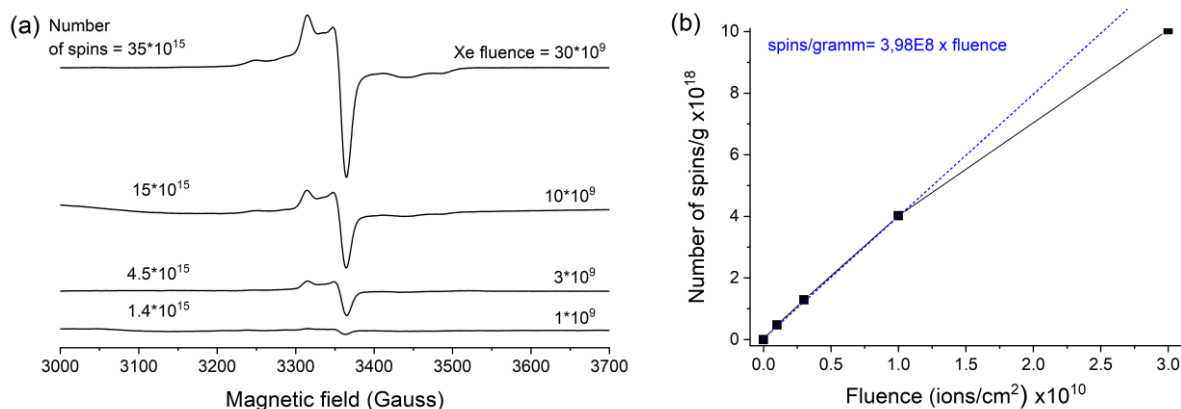


Figure 1. (a) EPR spectra of PVDF foils irradiated with Xe (1.2 MeV/u) at fluences from 10^9 to 3×10^{10} ions/cm² and (b) their corresponding number of radicals normalized by weight. All spectra were recorded at 200 K

Figure 1 (b) shows the dependence of the total number of radicals on ion fluence. Up to the fluence of 10^{10} ions/cm², a linear dependence is observed, followed by a deviation at higher fluences. Given the sample weight, polymer density and film thickness, the radical yield was found to be approximately equal to 6×10^5 radicals per Xe ion. Spectral analysis allowed the identification of three types of radicals. These were: peroxy ($-\text{CH}_2-\text{CFOO}^{\bullet}-\text{CH}_2-$), exhibiting the largest amplitude and accounting for approximately half of the total radical population; polyenyl ($-\text{CH}=\text{C}^{\bullet}-\text{CH}_2-$) detected upon annealing (at room temperature under Ar atmosphere) as the number of peroxide radicals decreases; and alkyl in-chain/end-chain with single or double C-C/C=C bonds, exhibiting a broad, poorly structured spectrum, which constitute the remaining half of the total radical population [21–23]. An unexpected finding was the significant presence of peroxy radicals despite all the precautions taken to minimize the irradiated foil exposure to air. A possible explanation is the high amount of pre-adsorbed oxygen present in the foil prior to irradiation, which immediately reacts with the newly formed radical species.

These combined radiation-induced effects, including unsaturations as well as a free volume formed upon gas molecule production, make the latent tracks susceptible to chemical attack, allowing transformation into a porous structure.

Chemical Etching of Xe-Irradiated PVDF Foils

In this work, chemical etching of Xe-irradiated PVDF foils was carried out in a concentrated potassium hydroxide solution (10 M) in the presence of potassium permanganate as an oxidizing agent at 65 °C. Pioneering works conducted in the 1980s by Tretyakova and Shirkova on etching of heavy ion tracks in various fluoropolymers demonstrated that PVDF could be effectively etched using an excess of potassium permanganate under alkaline conditions [18, 24]. Grasselli and Betz [25] studied the effect of KOH concentration on the etching process. Their work, conducted in the presence of 0.25 M KMnO_4 , demonstrated that high alkali concentration (9 M KOH) was essential for achieving well-defined porous structures. Additionally, it was demonstrated that etching temperatures between 55 and 65 °C were optimal for producing cylindrical pores. In contrast, higher temperatures (>85 °C) resulted in conical-shaped pores and lower temperatures (<50 °C) significantly slowed the chemical attack. For this reason the etching temperature in the current study was maintained in the range 60–65 °C.

The etching process was postulated to involve two consecutive steps [25]. The first step is an initial dehydrofluorination of the polymer structure induced by the alkaline environment, leading to the formation of C=C double bonds. The second step is the subsequent oxidative degradation of these double bonds by permanganate; this results in soluble low molecular weight compounds that are removed from the track regions. Indeed, due to the high electronegativity of fluorine, which “pulls” electron density away from neighboring carbon atoms, a high concentration of alkali catalyzes the dehydrofluorination of PVDF, resulting in the formation of $-\text{CH}=\text{CF}-$. In concentrated alkali, KMnO_4 acts as a strong oxidizing agent capable of breaking C=C bonds and oxidizing them to carboxylic acid salts (for primary and secondary carbons). A double bond at a carbon in the tertiary position (for instance, in cross-linked track halo) oxidizes to ketones and carboxylic acid salts.

In this work, an attempt was made to lower the potassium permanganate concentration while retaining the same track etching efficiency, thereby optimizing the process from both technical and economic perspectives. Figure 2 (a) illustrates the effect of KMnO_4 concentration in 10 M KOH aqueous solution on track etching rate.

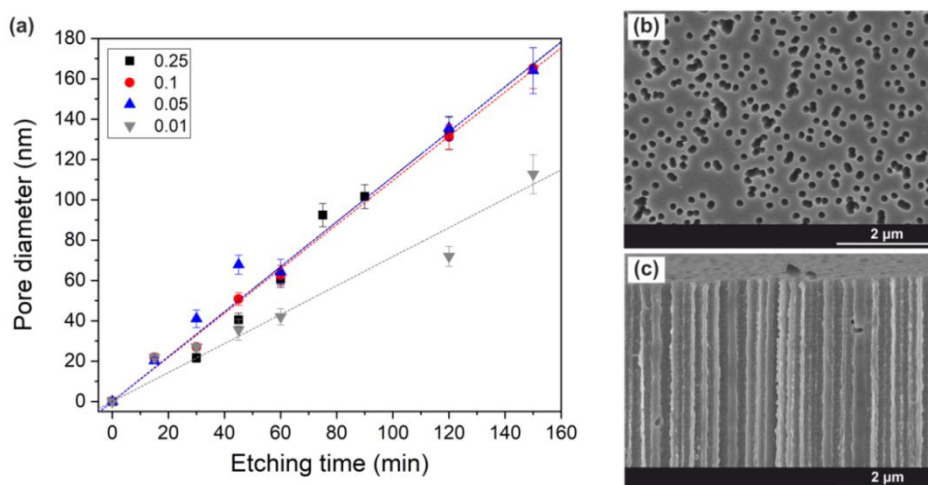


Figure 2. (a) Track etching rate of Xe-irradiated PVDF films as a function of KMnO_4 concentration in 10 M KOH aqueous solution. SEM images of (b) surface and (c) cross-sectional views of the sample etched in 0.05 M KMnO_4 (10 M KOH) at 63.5 °C for 120 min. Ion fluence: 10^9 ions/cm²

Prior to foil immersion in the etching solutions, they were pre-heated to correspond to the set etching temperature, ensuring consistent treatment conditions (63.5 °C). The track etching rate decreased from 1.1 nm/min to 0.7 nm/min when the KMnO_4 concentration was reduced from 0.25 to 0.01 M, respectively. However, varying the permanganate concentration within the range of 0.25–0.05 M did not cause any significant difference. Notably, the best linear fit correlation was found for 0.1 M KMnO_4 , indicating optimal process stability and reproducibility. Consequently, this concentration was selected for the fabrication of TMs in subsequent experiments.

Figures 2 (b) and (c) present SEM images of irradiated PVDF films etched in 10 M KOH with 0.05 M KMnO_4 . The cross-sectional view clearly demonstrates the formation of through cylindrical channels under these etching conditions. These results confirm that the permanganate concentration can be reduced fivefold without sacrificing pore quality and presents a direct optimization of the process established in [25]. Beyond the evident economic and environmental benefits, the reduction of oxidizer concentrations can mitigate non-selective background oxidation, potentially affecting the membrane surface chemistry.

Radiation Grafting of AA Within Nanopores of PVDF TMs

Radiation-induced graft polymerization of AA onto etched tracks was carried out through pre-irradiation method. More specifically, a polymer substrate was irradiated under inert atmosphere and grafting reaction was initiated by radicals remained in the post-etched tracks. As seen from EPR results, the initiators of grafting include a mixture of alkyl radicals and their oxidized species. In earlier work [26] it was demonstrated that the integral amount of radicals trapped within PVDF etched tracks decays exponentially with etch time. The reason for such a decrease is that the longer the etching process, the larger the pores are formed, the less trapped radicals in track wall are remained. Grafting yield (GY), calculated as a weight of the grafted polymer over a weight of substrate (expressed in wt.%), for the studied allyl monomer rises as pore size enlarges up to the etch time of 35 min. This is followed by a decrease as the etch time exceeds 40 min. A 60 % radical consumption seen for TMs with a given pore size was accompanied with graft polymerization. Although, the first reports on AA grafting in heavy ion tracks were made about twenty years ago [27, 15], the understanding of effects affecting on grafting process of AA is still far from being complete. The following subsections will focus on key graft polymerization parameters, such as the effect of inhibitor, monomer concentration, reaction temperature, and time.

Effect of Homopolymerization Inhibitor

The radiation grafting procedure involved immersing freshly etched nanoporous PVDF track-etched membranes (TMs) in aqueous solutions of acrylic acid (AA) monomer, followed by degassing and thermostating at 60 °C. Elevated temperature enhances the mobility of trapped radicals, improving their accessibility to the monomer. Simultaneously, it facilitates monomer diffusion toward active sites. However, these conditions also promote thermal homopolymerization of AA in solution, even when the monomer retains its standard stabilizer (MeHQ). Homopolymerization increases solution viscosity, limiting monomer availability and access to active sites within the nanopores. AA, like other acrylates, undergoes chain transfer reactions and exhibits fast polymerization kinetics, making GY control difficult.

To mitigate homopolymerization and slow down AA reactivity, ammonium ferrous sulfate (Mohr's salt) was employed. To emphasize the inhibition effect of Mohr's salt, a monomer concentration of 75 vol.% in water was chosen. This concentration was selected because the grafting rate is the fastest under such conditions and accompanied by a drastic expansion in the sample volume. Figure 3 illustrates the effect of Mohr's salt concentration on GY. The addition of the smallest quantity of Mohr's salt (0.05 %) caused a sharp decline in GY, reducing it by ca. 19 wt.% compared to inhibitor-free conditions (150 wt.%). Further increase in inhibitor concentration (0.1–0.5 %) resulted in a plateau, where GY remained largely unaffected by the additional inhibitor concentration increase. Mohr's salt acts as a radical scavenger through an electron transfer from Fe^{2+} to free radicals ($\text{Fe}^{2+} + \text{R}^{\bullet} \rightarrow \text{Fe}^{3+} + \text{R}^{-}$), terminating both homopolymerization in the bulk solution and graft initiation at accessible radical sites. The drastic GY reduction at 0.05 % suggests efficient quenching of free radicals in the bulk solution and those in close proximity to the nanopore surface. The subsequent plateau reflects the radicals that remain shielded within the nanopore interior. There, steric hindrance and restricted diffusion limit Fe^{2+} penetration, thereby preserving grafting activity. This spatial heterogeneity in radical accessibility, with surface radicals being quenched while pore-confined radicals remain active, could explain the observed GY leveling-off at higher inhibitor concentrations.

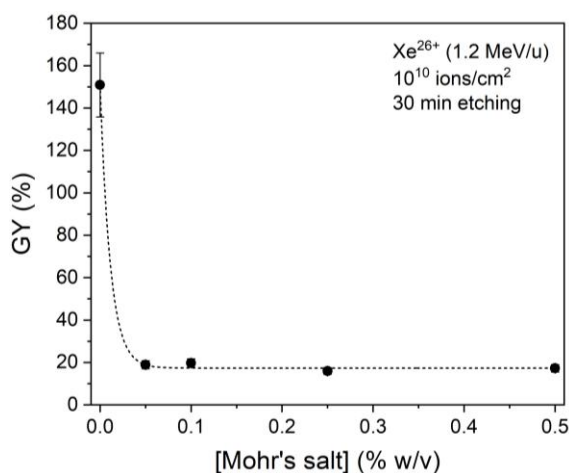


Figure 3. Dependence of the grafting yield (GY) on the Mohr's salt concentration (0–0.5 % w/v) in 75 vol.% AA aqueous solutions. Reaction conditions: 60 °C, 30 min

Effect of Temperature and Monomer Concentration

The effect of reaction temperature on AA grafting was investigated at 55, 60, 65, and 70 °C. Higher temperatures typically enhance monomer diffusion and radical mobility within the polymer matrix, thereby accelerating grafting kinetics. However, the results revealed an optimal temperature range rather than a monotonic increase. GYs were comparable at 55 and 60 °C, representing the highest efficiency. Increasing the temperature to 65 °C resulted in a moderate decrease, and further elevation to 70 °C produced the lowest GY (not shown). Such temperature-dependent behavior indicates that excessive heating promotes competing processes. These include radical recombination (termination reactions) and thermal homopolymerization in solution, which reduce the availability of both radicals and monomer for grafting. Consequently, 60 °C was identified as the optimal temperature, providing an effective balance between enhanced diffusion kinetics and minimized side reactions. This is consistent with the range reported in [10] for AA grafting onto PVDF films.

Figure 4 (a) illustrates the effect of AA concentration (10–100 vol.% in water) on grafting efficiency, examined at 60 °C in the presence of 0.25 % Mohr's salt over 30 minutes reaction time. GY increased steadily with AA concentration up to 50 vol.%, followed by a significant enhancement at 75 vol.%, before declining at 100 vol.%. The observed trend with the maximum GY of ~22 % aligns with the behavior reported for electron-beam grafted PVDF films [12] and reflects the dual role of water in the grafting system.

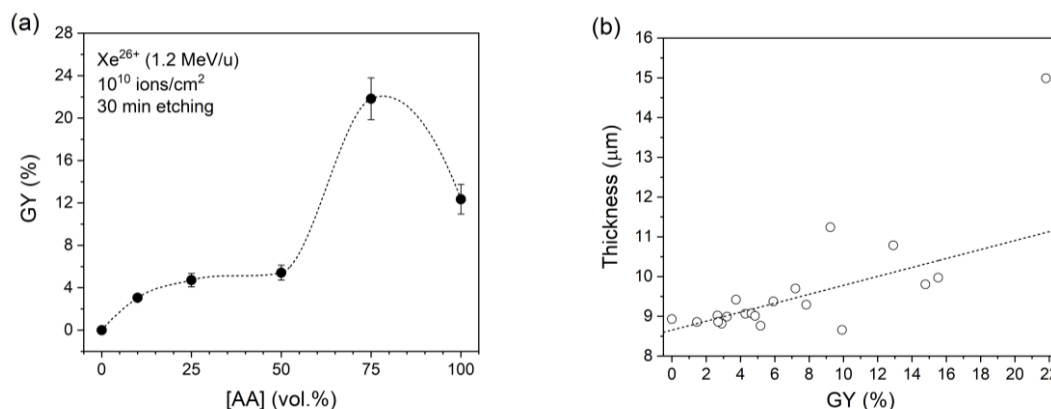


Figure 4. (a) Dependence of the grafting yield (GY) on the AA concentration in water. (b) Variation of sample average thickness as a function of GY. Mohr's salt concentration is 0.25 % w/v. Reaction conditions: 60 °C, 30 min

It serves not only as a solvent that facilitates monomer diffusion through the developing grafted polymer layer but also acts as a plasticizer for the PVDF, enhancing polymer chain mobility and accessibility of radical sites. Indeed, PVDF is a semi-crystalline polymer, and radicals generated during SHI irradiation can be localized in amorphous, crystalline or at the boundaries of crystalline/amorphous zones. The latter ones are expected to exhibit longer life-times, with their role in initiating graft polymerization being more significant than the radicals in amorphous zones. For continuous grafting, the monomer diffusion rate needs to be higher than the radical life-time. Furthermore, the monomer concentration must exceed its consumption during initiation and propagation. These factors, coupled with the enhanced swelling of PVDF in concentrated AA solutions (75 and 100 vol.%) [27], explain the observed grafting behavior. The decrease in GY at 100 vol.% AA aligns with literature reports indicating that PAA exhibits poor solubility in its monomer, leading to predominantly surface grafting rather than polymerization in bulk [10, 27].

Figure 4 (b) shows the correlation between GY and grafted membrane thickness. A GY of ~15 % from 100 vol.% AA results in approximately a 10 % thickness increase compared to the unmodified TM. In contrast, a GY of ~22 % from 75 vol.% AA led to about 60 % thickness expansion. This confirms that optimal water content is essential for achieving efficient pore-confined grafting. Based on these findings, pure AA is more suitable for achieving pore surface-localized functionalization. Diluted monomer solutions (≤ 50 vol.%) promote pore wall grafting. Meanwhile, higher monomer concentrations (51 to 99 vol.%) enhance bulk graft polymerization throughout the pore walls, spreading into the bulk membrane structure.

Kinetics of Grafting

Figure 5 exhibits the grafting kinetics of AA to PVDF TMs in 50 and 75 vol.% AA solutions containing 0.25 % Mohr's salt at 60 °C. As shown, the GY progresses through two distinct phases: (I) a rapid increase with a maximum at 30–45 min, followed by (II) a gradual decline and asymptotic saturation at longer reaction times. This behavior persisted across monomer concentrations and was initially attributed to diffusion-controlled inhibitor effects. However, identical behavior was observed in diluted AA solutions (≤ 50 vol.%) without any Mohr's salt.

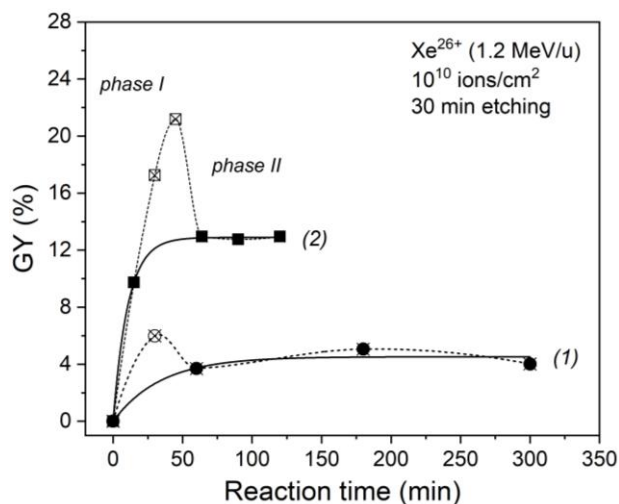


Figure 5. Grafting kinetics of AA to PVDF TMs at 60 °C. AA concentration is 50 (1) and 75 vol.% (2). Mohr's salt concentration is 0.25 % w/v. The spline connection of the experimental data highlights the behavior

During phase I, grafting acceleration arises from synergistic factors: (i) abundant radicals at pore surfaces initiate polymerization, (ii) unhindered AA diffusion into nanopores of water-plasticized PVDF, and (iii) hydrogen bonding between carboxyl groups of grafted PAA chains and incoming AA monomers, which locally enriches monomer concentration near reactive sites. These effects collectively maximize grafting efficiency during the initial stage. Subsequently, the observed decline (phase II) reflects both radical decay due to temperature-mediated recombination and consumption through grafting reactions. The apparent GY_{max} (empty crossed symbols) may be attributed to methodological artifacts: thermal polymerization of residual AA (diffused into PAA-g-PVDF) during post-grafting Soxhlet extraction in boiling water, inflating early GY measurements. This hypothesis was confirmed by using a more optimal washing procedure on grafted membranes. They were first soaked in water at room temperature for 12 hours, followed by extraction in boiling water. At longer reaction times, residual monomer diminishes. This leaves covalently grafted PAA as the primary contributor to the asymptotic plateau, which reflects a dynamic equilibrium between reduced grafting due to diffusion barriers and extractable homopolymer formation. The consistent behavior in inhibitor-free solutions confirms that pore confinement and post-processing artifacts are the primary drivers of the observed kinetic profile.

Characterization of PAA Nanopore-Grafted PVDF TMs

Figure 6 illustrates the FT-IR spectra of PVDF TMs before and after being grafted with PAA resulting in a GY of 22 %. The spectrum of pristine membrane (dashed line) includes: a doublet at 2985 and 3025 cm^{-1} corresponding to *sym* and *asym* stretching vibrations of CH_2 ; the bands at 1453, 1424, 1403, and 1385 cm^{-1} assigned to $\nu(\text{CH}_2)$ and $\nu(\text{C}-\text{C})$ vibrations; the intense bands at 1211 and 1183 cm^{-1} attributed to $\nu(\text{CF}_2)$ vibration; the absorption bands in the 1000–500 cm^{-1} range correspond to characteristic PVDF skeletal vibrations. Radiation grafting of PAA to PVDF TMs, conducted in 75 vol.% AA and 0.25 % w/v Mohr's salt at 60 °C, results in the appearance of a new absorption bands. These include a strong peak at $\sim 1710 \text{ cm}^{-1}$, assigned to $\text{C}=\text{O}$ stretching vibration in associated carboxyl groups (hydrogen-bonded) with a shoulder at $\sim 1750 \text{ cm}^{-1}$ corresponding to free carboxyl groups. The broad band in the 3500–2500 cm^{-1} range, associated with $\nu(\text{OH})$, is usually too weak in dried samples and superimposed with $\nu(\text{CH}_2)$ of PVDF. The low-intensity band at 1558 cm^{-1} is attributed to asymmetric vibration of carboxylate groups. This arises from partial dissociation of AA units under neutral pH conditions during grafting in aqueous media. Notably, treatment in dilute alkaline solutions transforms the dominant 1710 cm^{-1} (protonated carboxyl) into the 1558 cm^{-1} band (deprotonated carboxylate), and *vice versa*, confirming the pH-responsive behavior of grafted PAA.

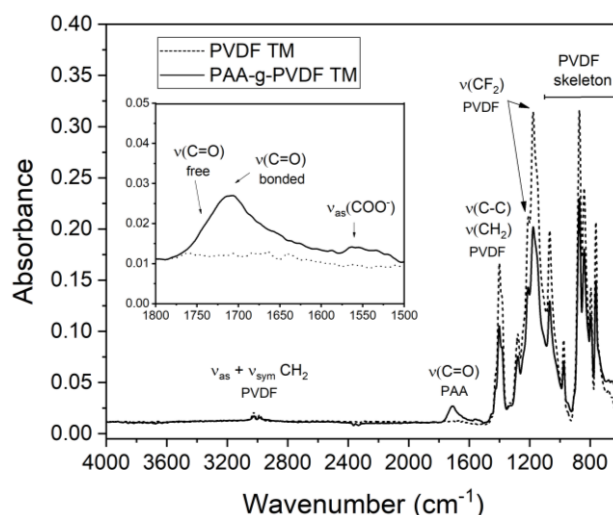


Figure 6. FT-IR spectra in ATR mode of PVDF TMs before and after PAA grafting (GY = 22 %). AA concentration: 75 vol.%. Mohr's salt concentration: 0.25 % w/v. Reaction conditions: 60 °C, 30 min

Surface chemical composition of samples grafted at various AA concentrations was analyzed by XPS. Figure 7 (a) shows a survey spectrum of non-modified PVDF TM, exhibiting characteristic F1s and C1s peaks with an F/C ratio of approximately 0.8. This reduced ratio (compared to pristine PVDF foil, F/C = 1.0) is attributed to radiation-induced dehydrofluorination during irradiation and latent track etching. Chemical etching selectively removes degraded polymer fragments from the latent tracks resulting in fluorine depletion overall the surface. After grafting in 75 % AA (Figure 7 (b)), XPS revealed a substantial increase in the O/F ratio from 0.1 to 0.6, demonstrating significant surface coverage by the grafted PAA layer.

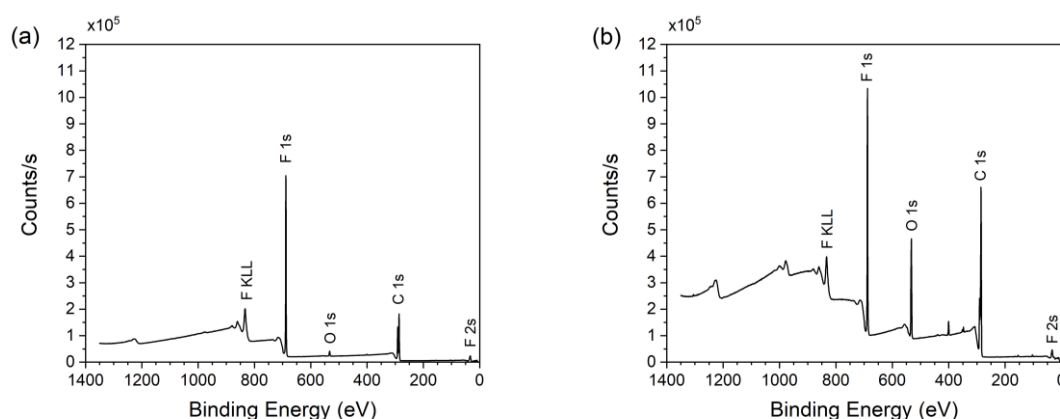


Figure 7. XPS survey spectra of PVDF TMs (a) before and (b) after PAA grafting (GY = 22 %). AA concentration: 75 vol.%. Mohr's salt concentration: 0.25 % w/v. Reaction conditions: 60 °C, 30 min

Table 1 summarizes atomic percentages for the PVDF TMs before and after PAA grafting depending on the monomer concentration and their GYs. When water was present in reaction solutions, the F/C ratio decreased progressively with increasing AA concentration, reaching a minimum at 75 vol.% AA. This indicates enhanced bulk functionalization, where growing PAA chains diffuse beyond nanopore confinement under optimal swelling conditions. This finding is consistent with the maximal membrane thickness expansion observed in Figure 4 (b).

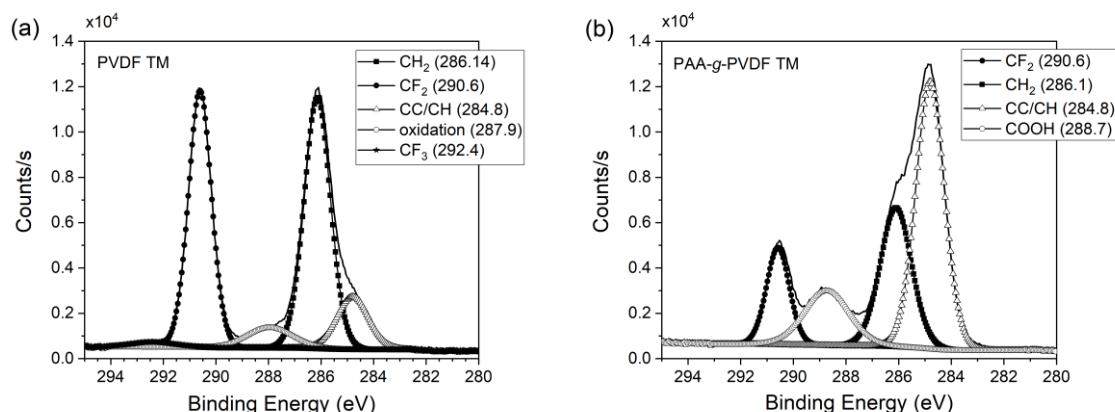


Figure 8. XPS C1s deconvoluted spectra of PVDF TMs (a) before and (b) after PAA grafting (GY = 22 %).

Table 1

Atomic composition of PAA-g-PVDF TMs

Sample	C1s (at.%)	F1s (at.%)	O1s (at.%)	F/C	O/F	GY (%)
PVDF TM	53.1	43.4	2.31	0.8	0.1	0
PAA-grafted PVDF TMs at varied [AA]						
10 vol.%	55.1	32.3	4.0	0.6	0.1	3.2
25 vol.%	56.2	38.5	4.0	0.7	0.1	4.3
50 vol.%	55.4	39.3	4.0	0.7	0.1	5.9
75 vol.%	62.7	21.4	12.4	0.3	0.6	21.8
100 vol.%	54.0	42.0	3.0	0.8	0.1	14.8

C1s regional spectra (Figure 8 (a)) for most grafted samples resembled pristine PVDF, confirming limited surface modification. In contrast, the sample grafted in 75 vol.% AA (Figure 8 (b)) showed pronounced carboxyl signatures (O–C=O at 288.7 eV). PVDF TMs grafted in 100 vol.% AA retained an F/C ratio identical to unmodified TMs, confirming strictly localized (nanopore-surface-only) modification. These results align with reported studies of PAA grafting onto electron-beam-irradiated PVDF foils [12].

Figure 9 depicts DSC curves revealing structural changes in PVDF foils induced by sequential processing, with key parameters summarized in Table 2. The pristine PVDF exhibits a characteristic endothermic melting peak, T_m , at 175.7 °C with an enthalpy of 49.0 J/g. Given the enthalpy of melting for fully crystalline PVDF ($\Delta H_{100\%} = 104.7$ J/g) [28], the crystallinity degree, χ_c , found as $\Delta H_m / \Delta H_{100\%} \times 100\%$ is estimated to be 46.8 %. Irradiation slightly reduces crystallinity while increasing the melting temperature (T_m) from 175.7 to 178.3 °C. This T_m increase is a due to radiation-induced cross-linking, restricting chain mobility and suppressing relaxation processes [29, 30]. Subsequent chemical etching restored T_m to 175.8 °C, confirming the selective removal of the radiation-damaged polymer from the latent tracks. After PAA grafting, T_m shifts to 177.6 °C. This shift is possibly due to two factors: (i) constrained PVDF chain mobility from interfacial PAA, and (ii) temperature-mediated radical recombination, inducing cross-links during graft polymerization. The observed reduction in χ_c with increasing GY is a well-documented phenomenon. Our results, showing a drop from 46.4 % to 30.6 %, align with the trends reported for other grafted systems, such as methyl methacrylate- and styrene-grafted PVDF [11, 31]. Such a behavior evidences the disruption of crystallites by the growing polymer grafts, initiated at the crystalline/amorphous boundaries. The consistency of this effect across different monomers and grafting methods confirms that the structural consequences of grafting are universal, thereby validating our findings. Additional transitions were observed. An exothermic transition near –40 °C (close to T_g of PVDF) points out nanoscale phase separation between flexible PVDF domains and glassy PAA ($T_g \approx 100$ °C). A broad endotherm at approximately 60 °C reflects dehydration of PAA-grafted samples.

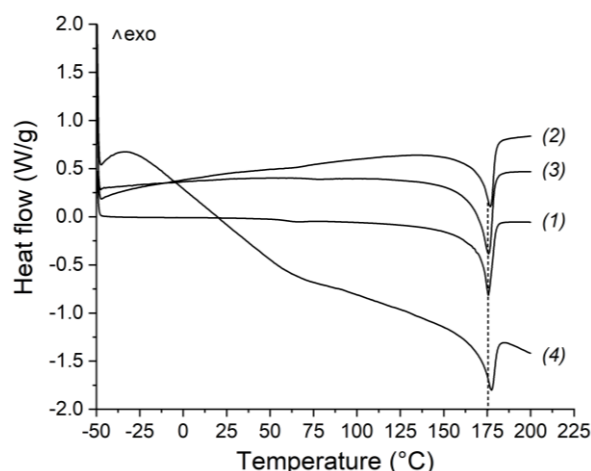


Figure 9. DSC curves for pristine PVDF (1), Xe-irradiated PVDF (2), PVDF TM (3), and PAA-g-PVDF TM (GY = 22 %) (4). AA concentration: 75 vol.%. Mohr's salt concentration: 0.25 % w/v. Reaction conditions: 60 °C, 30 min

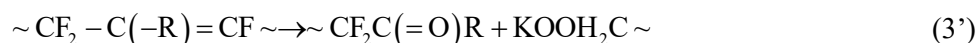
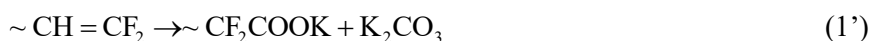
Table 2

Melting temperature (T_m), enthalpy of melting (ΔH_m), and crystallinity degree (χ_c) derived from DSC for pristine, Xe-irradiated, etched and AA-grafted PVDF TMs

Sample	T_m (°C)	ΔH_m (J/g)	χ_c (%)
PVDF	175.7	49.0	46.8
PVDF-Xe	178.3	48.5	46.3
PVDF TM	175.8	48.6	46.4
PAA-g-PVDF TM	177.6	32.0	30.6

Contact angle measurements confirm the progressive modification of the surface across different processing stages. Pristine PVDF foil exhibited a contact angle of $80 \pm 5^\circ$. Etched membranes showed significant hydrophilization, reducing the contact angle to $65 \pm 2^\circ$, attributed to carboxyl group formation. Following PAA grafting, contact angles modestly decreased across all AA concentrations, reaching $57 \pm 6^\circ$ for membranes grafted in 100 vol.% AA. Despite PAA's inherent hydrophilicity, this relatively small reduction confirms that wetting is primarily governed by nanometer-scale pore openings rather than bulk or surface functionalization.

Zeta-potential measurements provide valuable insights into the surface chemistry and nanoscale functionalization of PVDF TMs. As seen in figure 10, unmodified PVDF TMs exhibit a pH-independent negative charge ($\zeta \approx -20$ mV across pH 3–8). This can be attributed to carboxylic acid groups (fluorinated and not) and ketones formed upon oxidative cleavage of C=C in various positions:



To demonstrate the versatility of the pore-confined grafting approach beyond PAA, poly(4-vinylpyridine) (P4VP), a cation-exchange polymer exhibiting pH-dependent charge behavior, was grafted to PVDF TMs. Its inverse charge modulation verifies that the interfacial properties are governed solely by the grafted polymer. Upon P4VP grafting, the charge behavior changes dramatically. Below pH 5.2, protonation causes a strong positive potential ($\zeta \approx +20$ mV at pH 3). Above pH 5.2, deprotonation restores a negative charge ($\zeta \approx -20$ mV at pH 8). The isoelectric point (IEP) of 5.2 found for the P4VP-g-PVDF TMs is consistent with the dissociation constant of pure P4VP [32]. The complete counterbalancing of the negative membrane charge emphasizes a uniform and continuous grafted P4VP layer that governs the interfacial behavior without interference from the substrate. This ability to precisely engineer the surface charge of the nanopores is crucial for advanced applications such as charge-selective separation, nanofluidic devices, and sensors.

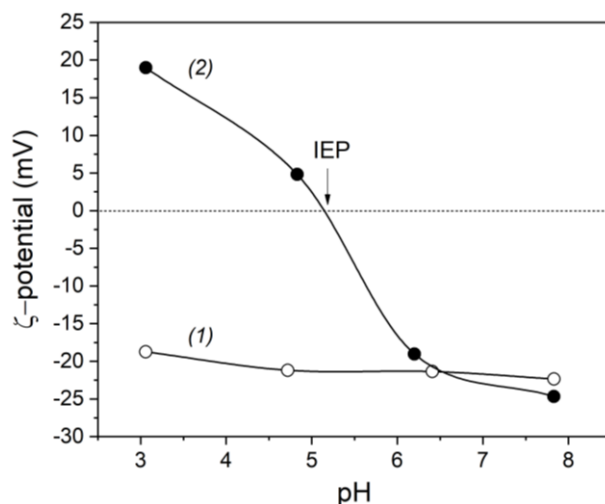


Figure 10. Zeta-potential of PVDF TMs before (1) and after (2) grafting with P4VP (GY = 1.6 %, fluence of 10^9 ions/cm²) as a function of pH

Confocal laser fluorescence microscopy was employed to visualize the location of grafted polymer. This was achieved by detecting Rhodamine 6G (Rh6G), a fluorescent agent that binds to carboxylic acid groups of the grafted PAA chains. To distinguish between grafted PAA and carboxyl groups introduced by PVDF oxidation during chemical etching, a control experiment was performed. Prior to grafting, freshly prepared membranes were treated with EDC/NHS (2:1 molar ratio) in 0.1 M acetate buffer (pH 5.0), followed by coupling with ethylenediamine (EDA) in PBS (pH 7.4). These carboxyl-deactivated samples were then subjected to PAA in 100 vol.% AA to ensure grafting occurred exclusively from pore surfaces. Figure 11 presents the photoluminescence surface mapping of PAA-g-PVDF TMs before and after Rh6G sorption.

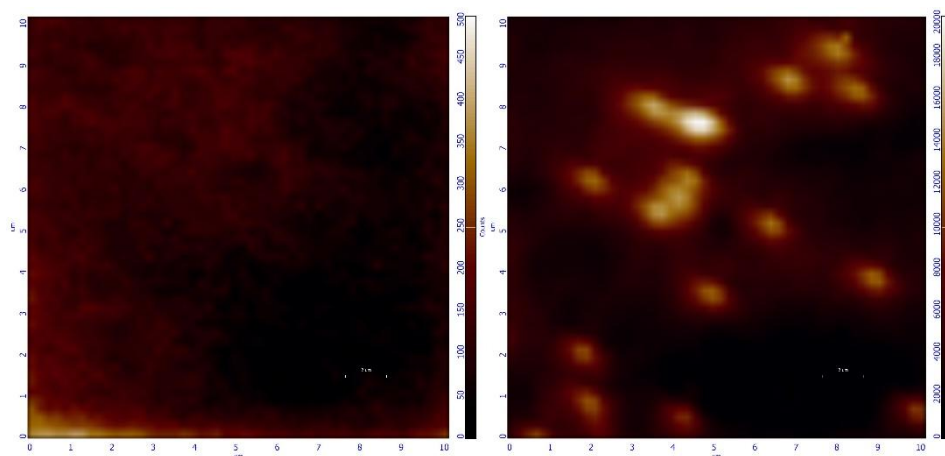


Figure 11. Photoluminescence surface mapping of PAA-g-PVDF TMs before (left) and after (right) sorption of Rhodamine 6G. Grafting was performed in 100 vol.% AA onto PVDF TMs with the fluence of 10^7 ions/cm². Intensity scales: 0–500 and 0–20,000 counts for left and right images, respectively. Scale bars: 2 μ m

Although PVDF exhibits intrinsic luminescence and Rh6G adsorbs nonspecifically on membrane surface, both contributing to background luminescence, the intense pore-localized signal contrasts sharply with the surrounding matrix. This spatial contrast, combined with pore density matching the ion fluence, clearly confirms nanopore-confined grafting.

Conclusions

Pore-localized functionalization of nanoporous PVDF TMs has been achieved through radiation-induced graft polymerization of AA monomer. Cylindrical through nanopores were produced by irradiation with energetic xenon ions under optimized alkaline oxidative etching, retaining residual radical sites along the ion tracks. These radical sites eliminate the need for external initiators or activation, enabling direct initi-

ation of polymerization reaction exclusively within the nanopores. Grafting efficiency was demonstrated through optimization of inhibitor concentration, monomer concentration, reaction temperature and time.

FT-IR and XPS analyses revealed a covalent attachment of PAA to PVDF TMs while its efficiency towards bulk *versus* surface modification is mainly governed by the monomer/solvent ratio. When growing PAA chains can diffuse beyond the etched track confinement under optimal polymer substrate swelling conditions, a significant decrease in the crystallinity of the grafted samples was observed by DSC. This was attributed to the crystallite disruption by PAA grafts initiated at crystalline/amorphous boundaries. Furthermore, the assessment of zeta-potentials provided a valuable insight into the surface chemistry and confirmed a continuous pore functionalization resulted in a complete counterbalancing of the negatively charged pore walls when cation-exchange P4VP chains are grafted. Confocal fluorescence microscopy enabled the visualization of PAA-grafted nanopores by detecting the luminescence of Rhodamine 6G adsorbed onto the carboxyl groups, illustrating that the grafted polymer is confined to the pore interiors.

The presented findings illustrate the potential of radiation-induced grafting as a powerful technique for tailoring the surface chemistry of nanoporous membranes at the nanoscale. This approach offers a platform for creating nanoporous membranes with tunable characteristics for energy, biomedical, and separation applications, opening new possibilities for spatially-controlled functionality in advanced materials.

Funding

This work was supported by Sistema Public Joint Stock Financial Corporation (grant No. 801/39-24) and JINR-SA Project JINR23030981618 (grant No. 1004). The EPR studies were conducted within the framework of State Assignment No. 124013100858-3.

*Author Information**

**The authors' names are presented in the following order: First Name, Middle Name and Last Name*

Angelina Viktorovna Kryukova-Seliverstova — Master student, Department of Nanotechnology and New Materials, Dubna State University, Universitetskaya Street, 141980, Dubna, Russia; e-mail: angelina3082001@gmail.com

Oleg Leonidovich Orelovich — Head of Electron Microscopy Group, Flerov Laboratory of Nuclear Reactions, Joint Institute for Nuclear Research, Joliot-Curie Street, 141980, Dubna, Russia; e-mail: orel@jinr.ru; <https://orcid.org/0000-0002-8786-1828>

Vladimir Alekseevich Altynov — Research Scientist, Flerov Laboratory of Nuclear Reactions, Joint Institute for Nuclear Research, Joliot-Curie Street, 141980, Dubna, Russia; e-mail: altynov@jinr.ru; <https://orcid.org/0000-0001-6247-8884>

Alexander Vladimirovich Akimov — Leading Researcher, Laboratory for Physical Methods of Functional Materials Research, Federal Research Center of Problems of Chemical Physics and Medicinal Chemistry RAS, Academician Semenov Avenue, 142432, Chernogolovka, Russia; e-mail: shura@icp.ac.ru; <https://orcid.org/0000-0001-6159-439X>

Alexander Sergeevich Shmakov — Research Assistant, Laboratory for Physical Methods of Functional Materials Research, Federal Research Center of Problems of Chemical Physics and Medicinal Chemistry RAS, Academician Semenov Avenue, 142432, Chernogolovka, Russia; e-mail: shmakovchem@mail.ru; <https://orcid.org/0009-0009-8084-0088>

Daria Vladimirovna Nikolskaya — Process Engineer, Flerov Laboratory of Nuclear Reactions, Joint Institute for Nuclear Research, Joliot-Curie Street, 141980, Dubna, Russia; e-mail: nikolskaya@jinr.ru; <https://orcid.org/0009-0004-2181-1002>

Nikita Sergeevich Kirilkin — Junior Research Scientist, Flerov Laboratory of Nuclear Reactions, Joint Institute for Nuclear Research, Joliot-Curie Street, 141980, Dubna, Russia; e-mail: kirilkin@jinr.ru; <https://orcid.org/0000-0003-3782-0515>

Uliana Vladimirovna Pinaeva (*corresponding author*) — Research Scientist, Flerov Laboratory of Nuclear Reactions, Joint Institute for Nuclear Research, Joliot-Curie Street, 141980, Dubna, Russia; e-mail: pinaeva@jinr.ru; <https://orcid.org/0000-0003-1724-6149>

Author Contributions

The manuscript was prepared with contributions from all authors, and all authors have approved the final version for submission. **CRedit**: **Angelina Viktorovna Kryukova-Seliverstova** investigation, formal analysis, visualization, writing — original draft; **Oleg Leonidovich Orelovich** investigation, formal analysis; **Vladimir Alekseevich Altynov** — investigation, formal analysis; **Alexander Vladimirovich Akimov** conceptualization, methodology, formal analysis; **Alexander Sergeevich Shmakov** investigation, writing — original draft; **Daria Vladimirovna Nikolskaya** investigation, resources; **Nikita Sergeevich Kirilkin** investigation, formal analysis; **Uliana Vladimirovna Pinaeva** conceptualization, methodology, investigation, formal analysis, writing — review & editing, supervision.

Acknowledgments

Authors gratefully acknowledge Oleg M. Ivanov for performing the irradiation of PVDF foils and for his insightful contributions to discussions during this research.

Conflicts of Interest

The authors declare no conflict of interest.

References

- 1 Nasef, M. M., & Güven, O. (2012). Radiation-grafted copolymers for separation and purification purposes: Status, challenges and future directions. *Progress in Polymer Science*, 37(12), 1597–1656. <https://doi.org/10.1016/j.progpolymsci.2012.07.004>
- 2 Saxena, P., & Shukla, P. (2021). A comprehensive review on fundamental properties and applications of poly (vinylidene fluoride)(PVDF). *Advanced Composites and Hybrid Materials*, 4(1), 8–26. <https://doi.org/10.1007/s42114-021-00217-0>
- 3 Costa, C. M., Cardoso, V. F., Pedro, M., Correia, D. M., Gonçalves, R., Costa, P., Correia, V., Ribeiro, C., Fernandes, M. M., Martins, P. M., & Lanceros-Méndez, S. (2023). Smart and multifunctional materials based on electroactive poly (vinylidene fluoride): recent advances and opportunities in sensors, actuators, energy, environmental, and biomedical applications. *Chemical reviews*, 123(19), 11392–11487. <https://doi.org/10.1021/acs.chemrev.3c00196>
- 4 Apel, P. Y. (2019). Fabrication of functional micro-and nanoporous materials from polymers modified by swift heavy ions. *Radiation Physics and Chemistry*, 159, 25–24. <https://doi.org/10.1016/j.radphyschem.2019.01.010>
- 5 Ma, T., Janot, J. M., Balme, S. (2020). Track-etched nanopore/membrane: from fundamental to applications. *Small Methods*, 4(9), 2000366. <https://doi.org/10.1002/smt.202000366>
- 6 Barsbay, M., & Güven, O. (2014). Grafting in confined spaces: Functionalization of nanochannels of track-etched membranes. *Radiation Physics and Chemistry*, 105, 26–30. <https://doi.org/10.1016/j.radphyschem.2014.05.018>
- 7 Chapiro, A. (1959). Préparation des copolymères greffés du polytétrafluoroéthylène (Teflon) par voie radiochimique. *Journal of Polymer Science*, 34(127), 481–501. <https://doi.org/10.1002/pol.1959.1203412735>
- 8 Dargaville, T. R., George, G. A., Hill, D. J. T., & Whittaker, A. K. (2003). High energy radiation grafting of fluoropolymers. *Progress in Polymer Science*, 28(9), 1355–1376. [https://doi.org/10.1016/s0079-6700\(03\)00047-9](https://doi.org/10.1016/s0079-6700(03)00047-9)
- 9 Chapiro, A. (1977). Radiation induced grafting. *Radiation Physics and Chemistry*, 9(1-3), 55–67. [https://doi.org/10.1016/0146-5724\(77\)90072-3](https://doi.org/10.1016/0146-5724(77)90072-3)
- 10 Ellinghorst, G., Niemöller, A., & Vierkotten, D. (1983). Radiation initiated grafting of polymer films — an alternative technique to prepare membranes for various separation problems. *Radiation Physics and Chemistry*, 22(3-5), 635–642. [https://doi.org/10.1016/0146-5724\(83\)90073-0](https://doi.org/10.1016/0146-5724(83)90073-0)
- 11 Betz, N. (1995). Ion track grafting. *Nuclear Instruments and Methods in Physics Research Section B Beam Interactions with Materials and Atoms*, 105(1-4), 55–62. [https://doi.org/10.1016/0168-583x\(95\)00911-6](https://doi.org/10.1016/0168-583x(95)00911-6)
- 12 Clochard, M.-C., Bégué, J.-P., Lafon, A., Caldemaison, D., Bittencourt, C., Pireaux, J. J., & Betz, N. (2004). Tailoring bulk and surface grafting of poly(acrylic acid) in electron-irradiated PVDF. *Polymer*, 45(26), 8683–8694. <https://doi.org/10.1016/j.polymer.2004.10.052>
- 13 Mazzei, R., Bermúdez, G. G., Betz, N., & Cabanillas, E. (2004). Swift heavy ion induced graft polymerization in track etched membranes' submicroscopic pores. *Nuclear Instruments and Methods in Physics Research Section B: Beam Interactions with Materials and Atoms*, 226(4), 575–584. <https://doi.org/10.1016/j.nimb.2004.08.001>
- 14 Mazzei, R., García Bermúdez, G., Camporotondi, D. E., Arbeitman, C., del Grosso, M. F., & Behar, M. (2012). New membranes obtained by grafted irradiated PVDF foils. *Nuclear Instruments and Methods in Physics Research Section B: Beam Interactions with Materials and Atoms*, 287, 26–30. <https://doi.org/10.1016/j.nimb.2012.05.040>
- 15 Mazzei, R., Betz, N., Bermúdez, G. G., Massa, G., & Smolko, E. (2005). Submicroscopic pores grafted using the residual sites produced by swift heavy ions. *Nuclear Instruments and Methods in Physics Research Section B: Beam Interactions with Materials and Atoms*, 236(1-4), 407–412. <https://doi.org/10.1016/j.nimb.2005.04.007>

- 16 Cuscito, O., Clochard, M. -C., Esnouf, S., Betz, N., & Lairez, D. (2007). Nanoporous β -PVDF membranes with selectively functionalized pores. *Nuclear Instruments and Methods in Physics Research Section B: Beam Interactions with Materials and Atoms*, 265(1), 309–313. <https://doi.org/10.1016/j.nimb.2007.08.089>
- 17 Barsbay, M., Güven, O., Bessbousse, H., Wade, T., Beuneu, F., & Clochard, M. -C. (2013). Nanopore size tuning of polymeric membranes using the RAFT-mediated radical polymerization. *Journal of Membrane Science*, 445, 135–145. <https://doi.org/10.1016/j.memsci.2013.05.029>
- 18 Tretyakova, S. P., Shirkova, V. V., Khitrova, N. B., & Borcea, C. (1986). Polyvinylidenefluoride (PVF) as a charged particle detector. *Nucl. Tracks Radiat. Meas.*, 12.
- 19 Balanzat, E., Bouffard, S., A. Le Moël, & Betz, N. (1994). Physico-chemical modifications induced in polymers by swift heavy ions. *Nuclear Instruments and Methods in Physics Research Section B Beam Interactions with Materials and Atoms*, 91(1-4), 140–145. [https://doi.org/10.1016/0168-583x\(94\)96204-9](https://doi.org/10.1016/0168-583x(94)96204-9)
- 20 Bogar, M. S., Beuermann, S., Dmitrieva, E., Drache, M., Gohs, U., Kunz, U., Lemmermann, T., Rosenkranz, M., Stehle, M., & Zschech, C. (2021). Quantitative EPR study of poly(vinylidene fluoride) activated by electron beam treatment. *Radiation Physics and Chemistry*, 184, 109421. <https://doi.org/10.1016/j.radphyschem.2021.109421>
- 21 Komaki, Y., Ishikawa, N., Morishita, N., & Takamura, S. (1996). Radicals in heavy ion-irradiated polyvinylidene fluoride. *Radiation Measurements*, 26(1), 123–129. [https://doi.org/10.1016/1350-4487\(95\)00286-3](https://doi.org/10.1016/1350-4487(95)00286-3)
- 22 Betz, N., Petersohn, E., & Le Moël, A. (1996). Free radicals in swift heavy ion irradiated fluoropolymers: An electron spin resonance study. *Radiation Physics and Chemistry*, 47(3), 411–414. [https://doi.org/10.1016/0969-806x\(95\)00127-j](https://doi.org/10.1016/0969-806x(95)00127-j)
- 23 Goslar, J., Hilczer, & B., Smogór, H. (2005). ESR studies of fast electron irradiated ferroelectric poly (vinylidene fluoride). *Acta Physica Polonica A*, 108(1), 89–94.
- 24 Tretyakova, S. P., & Jolos, L. V. (1978). Heavy ion particle track detector of fluoropolymers. *Prib. Tekh. Eksp.*, 1, 36–41.
- 25 Grasselli, M., & Betz, N. (2005). Making porous membranes by chemical etching of heavy-ion tracks in β -PVDF films. *Nuclear Instruments and Methods in Physics Research Section B: Beam Interactions with Materials and Atoms*, 236(1-4), 501–507. <https://doi.org/10.1016/j.nimb.2005.04.027>
- 26 Pinaeva, U., Dietz, T. C., Sheikhy, M. -Al., Balanzat, E., Castellino, M., Wade, T. L., & Clochard, M. -C. (2019). Bis[2-(methacryloyloxy)ethyl] phosphate radiografted into track-etched PVDF for uranium (VI) determination by means of cathodic stripping voltammetry. *Reactive and Functional Polymers*, 142, 77–86. <https://doi.org/10.1016/j.reactfunctpolym.2019.06.006>
- 27 Betz, N., Begue, J., Goncalves, M., K. Gionnet, G. Délérís, & A. Le Moël. (2003). Functionalisation of PAA radiation grafted PVDF. *Nuclear Instruments and Methods in Physics Research Section B: Beam Interactions with Materials and Atoms*, 208, 434–441. [https://doi.org/10.1016/s0168-583x\(03\)00900-5](https://doi.org/10.1016/s0168-583x(03)00900-5)
- 28 Zhou, Z., Li, W., He, T., Qian, L., Tan, G., & Ning, C. (2016). Polarization of an electroactive functional film on titanium for inducing osteogenic differentiation. *Scientific Reports*, 6(1). <https://doi.org/10.1038/srep35512>
- 29 Volgina, E., Pinaeva, U., Temnov, D., Ivanov, O., Mitrofanov, S., & Nechaev, A. (2025). Relaxation processes in swift heavy ion irradiated poly(vinylidene fluoride) films. *Radiation Physics and Chemistry*, 230, 112593. <https://doi.org/10.1016/j.radphyschem.2025.112593>
- 30 Betz, N., Petersohn, E., & Le Moël, A. (1996). Swift heavy ions effects in fluoropolymers: radicals and crosslinking. *Nuclear Instruments and Methods in Physics Research Section B: Beam Interactions with Materials and Atoms*, 116(1-4), 207–211. [https://doi.org/10.1016/0168-583x\(96\)00125-5](https://doi.org/10.1016/0168-583x(96)00125-5)
- 31 Percolla, R., Musumeci, P., Calcagno, L., Foti, G., & Ciavola, G. (1995). Grafting of styrene in polyvinylidene fluoride by high energy ion irradiation. *Nuclear Instruments and Methods in Physics Research Section B: Beam Interactions with Materials and Atoms*, 105(1-4), 181–185. [https://doi.org/10.1016/0168-583x\(95\)00636-2](https://doi.org/10.1016/0168-583x(95)00636-2)
- 32 Wang, H., Lee, I. H., & Yan, M. (2012). A general method to determine ionization constants of responsive polymer thin films. *Journal of Colloid and Interface Science*, 365(1), 178–183. <https://doi.org/10.1016/j.jcis.2011.08.081>